Subpicosecond photoconductivity of $In_{0.53}Ga_{0.47}As$: Intervalley scattering rates observed via THz spectroscopy

Stephen E. Ralph* and Yue Chen
Department of Physics, Emory University, Atlanta, Georgia 30322

Jerry Woodall and Dave McInturff
Department of Electrical and Computer Engineering, Purdue University, Lafayette, Indiana 47907

(Received 22 December 1995)

We report on the transient photoconductivity of hot carriers in undoped bulklike $In_{0.53}Ga_{0.47}As$ observed via time-resolved terahertz far-infrared spectroscopy. For very dilute photoexcitation densities of $<1\times10^{15}$ cm^{-3} and an initial excess carrier energy of 630 meV, we find that electrons have an effective intervalley $L\rightarrow\Gamma$ return time of 3.1 ps as measured via the increased electrical conductivity associated with Γ electrons. In contrast, a *total* conductivity risetime of $\sim$0.5 ps is observed for electrons with initial excess energy insufficient to cause intervalley scattering. The observed frequency dependent conductivity is analyzed via the Drude theory, allowing the determination of the temporal dynamics of the mobility at dilute excitation densities of $\sim1\times10^{14}$ cm^{-3}. [S0163-1829(96)05531-2]

I. INTRODUCTION

The transient transport dynamics of photoexcited carriers in semiconductors are of importance for understanding fundamental scattering phenomena and the creation of additional optical and electronic devices. Hot carriers, created either by optical excitation or electronic heating, undergo a number of energy-loss mechanisms including carrier-carrier scattering and longitudinal-optical (LO) phonon-scattering events. At high carrier densities both electron-electron and electron-hole scattering processes dominate, yielding a quasiequilibrium carrier distribution within a few tens of femtoseconds. At low carrier densities LO-phonon-cascade emission is believed to dominate. For III-V compound semiconductors, intervalley scattering events also occur via the interaction of large momentum phonons, and often dominate both transient and quasiequilibrium transport phenomena. Indeed, many electronic devices require intervalley scattering for operation. Intervalley scattering events are not limited to high-field phenomena, but include photonic interactions as well.

Traditionally, both time-resolved photoluminescence (PL) and transient absorption studies have provided the bulk of the experimental data on carrier cooling phenomena,[1,2] although a few cw experiments have been reported.[3] Time-resolved PL provides a direct measure of carrier energy relaxation rates in contrast to far-infrared (FIR) transmission, which provides a measure of the conductivity or momentum relaxation rate. More importantly, as pointed out by Ridley,[4] many scattering phenomena and quantum confinement effects are strongly influenced by the introduction of large carrier densities often encountered in time-resolved PL measurements. These high carrier densities add complexities including coupled-mode effects and the subsequent inability to observe the bare scattering interaction even in the bulk. On the other hand, the far infrared interacts preferentially with mobile charge and, as we demonstrate here using the short-pulse terahertz (THz) generation technique, can probe carrier transport phenomena at very low carrier densities with femtosecond temporal resolution. It is convenient to view the THz interaction as an examination of the local phase-space environment of the individual carrier states without the complexities of high carrier densities. Although the far infrared has been used for many years to characterize low-energy excitations in semiconductors, the THz generation technique and the subsequent ability to perform FIR studies with subpicosecond temporal resolution is just beginning to be exploited. Recent fundamental work in short-pulse FIR generation includes the study of the generation mechanism, the subpicosecond dynamics of photocarrier screening,[5] and the spectroscopic study of photoinduced conductivity in GaAs.[6] Each of these studies was performed at relatively large photoinjected carrier concentrations. We point out that there have been only a few reports using the terahertz generation technique as a spectroscopic method of probing the transient dynamics of low-energy excitations. In this paper, to our knowledge, we present the first time-resolved far-infrared spectroscopy study of the transient conductivity in $In_{0.53}Ga_{0.47}As$ ($In_xGa_{1-x}As$). Our technique allows the investigation of transport phenomena at very dilute carrier densities.

The interaction between the electromagnetic wave and the material can be described by the frequency- and time-dependent dielectric response function $\varepsilon(\omega,t)$, which can be represented as a sum of three contributions: (i) interband transitions including intersubband transitions, (ii) free-carrier effects, and (iii) the contribution of phonons. Due to the small excitation energy, the measurement is not sensitive to interband- or phonon-related transitions. Thus, for the transport studies presented here, we require only the free-carrier contribution. The complete dielectric response function is then

$$\varepsilon(\omega)=\varepsilon_0+\frac{i\sigma}{\omega\varepsilon_0}, \quad (1)$$

 © 1996 The American Physical Society

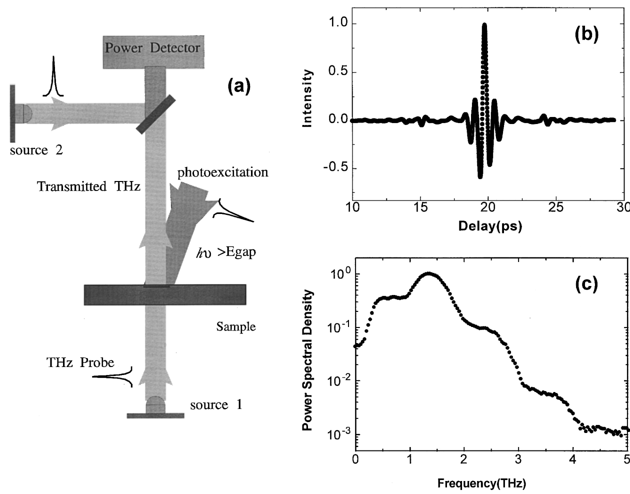

FIG. 1. (a) Femtosecond far-infrared spectrometer with sample photoexcitation. (b) Resulting reference interferogram and (c) the corresponding spectral power density.

where σ is the complex conductivity and, as represented in (1), is completely general. Material parameters, including the mobility μ and carrier density N, can be determined via an appropriate model of the conductivity. Our analysis employs the Drude theory, which results in the conductivity

$$\sigma(\omega)=i\varepsilon_0\omega_p^2/(\omega+i\Gamma_m), \qquad (2)$$

where ω_p is the plasma frequency, Γ_m is the carrier momentum scattering rate, and the other terms have their usual meaning. The conductivity can be related to the experimentally measured transmission data using the Fresnel coefficients for the multilayer semiconductor structure.[7] The terahertz spectroscopic system thus interacts preferentially with mobile charge species of $In_xGa_{1-x}As$, and is a direct measure of the sample conductivity. The time resolved capability of the pulsed FIR source allows the determination of both $\sigma(\omega,t)$ and, assuming an appropriate model of conduction, $N(t)$ and $\mu(t)$. The extension of these measurements to quantum-confined structures will be reported separately.

II. EXPERIMENT

Freely propagating terahertz radiation is generated via an ultrafast transient photocurrent. The FIR pulses, 200 fs in duration, are created via the photoexcitation of carriers within the large electric field developed between the externally biased electrodes fabricated on semi-insulating GaAs.[8] The resulting pulsed emission of FIR is comprised of a continuum of frequencies spanning from $\sim$0.1 to beyond 3 THz.

Figure 1(a) schematically depicts the THz spectroscopic system which allows the spectrally integrated or spectrally resolved FIR transmission study of materials. The time-resolved spectrally integrated transmission of the FIR THz beam is obtained via a pump-probe arrangement using only source 1, and the photoexcitation pump shown in Fig. 1(a) (i.e., THz source 2 and the beam splitter are not used). The total FIR power transmitted through the sample is measured using a liquid-helium-cooled bolometer. For our differential transmission technique, only the visible or near-infrared photoexcitation pump beam is mechanically chopped; the synchronously observed THz signal thus represents only that component of the THz beam which changes due to the photoexcitation. The spectral content of the transmitted THz pulse is obtained by fixing the relative delay between the photoexcitation pulse and the arrival of the THz probe pulse at the sample. The transmitted probe pulse is then combined with the THz beam of source 2 using the combining silicon beam splitter in the interferometer arrangement of Fig. 1(a). An interferogram,[9] Fig. 1(b), is obtained by scanning the relative delay of THz source 2 with respect to THz source 1. In this fashion, a sequence of interferograms is taken, each corresponding to a different delay between the photoexcitation source and the probe FIR pulse of source 1. Again, the signal is obtained by synchronous detection with respect to the chopped photoexcitation beam. This arrangement yields true differential spectroscopic data, and provides exceptional sensitivity allowing transmission changes to be observed to one part in 10^4. A Fourier analysis of the interferogram reveals the power spectral density of the transmitted pulse, Fig. 1(c), for any fixed delay with respect to the photoexcitation source. We note that useful power extends to 3 THz, which corresponds to 12.4 meV.

The dependence of the conductivity on the excess carrier energy is determined by use of a number of photoexcitation energies from 0.8 eV (1.55 μm) to 1.55 eV ($\sim$800 nm). The shorter-wavelength pulses near 800 nm are obtained from the same mode-locked Ti-sapphire laser which is used to generate the THz beams. The longer wavelengths ($>$1.30 μm) are produced from a parametric oscillator which is synchronously pumped with the Ti-sapphire laser. These longer-wavelength pulses maintain a pulse width of $<$100 fs and have less than 50-fs jitter with respect to the Ti-sapphire pulses. The THz probe beam produces a $\sim$5-mm-diam spot on the sample, and is fully enveloped by the 8-mm photoexcitation. The large photoexcitation area limits our temporal resolution to $\sim$500 fs, as confirmed by the measurement of low growth temperature GaAs (LT-GaAs) material.

The $In_xGa_{1-x}As$ samples used in this work are grown by molecular-beam epitaxy on Fe:InP substrates, and consist of a nominally undoped 1.0-μm-thick $In_xGa_{1-x}As$ light-absorbing layer followed by a 50-nm $Al_{0.52}In_{0.47}As$ cap layer. A 100-nm $Al_{0.52}In_{0.47}As$ buffer layer was used at the substrate interface. This heterojunction structure eliminates surface and substrate interface effects, and thus allows us to study the fundamental bulk phenomena. For each of the excitation wavelengths investigated, nearly all of the absorption occurs in the $In_xGa_{1-x}As$ layer, as determined by separate absorption measurements.

III. TRANSIENT FIR TRANSMISSION

The bare momentum scattering rates are examined via the transient conductivity at various excess electron energies for carrier densities $<10^{15}$ cm^{-3}. Figure 2 shows the change in transmission $|\Delta T/T|$ for two excitation wavelengths, $\lambda=810$ nm and 1.4 μm. Only the shorter-wavelength excitation provides the necessary excess electron energy for intervalley scattering. Note that increasing signal strength corresponds to an increasing conductivity and a decreasing transmission. At long delays, $\tau>50$ ps, the carriers have reached thermal equilibrium, and the near-exponential decay

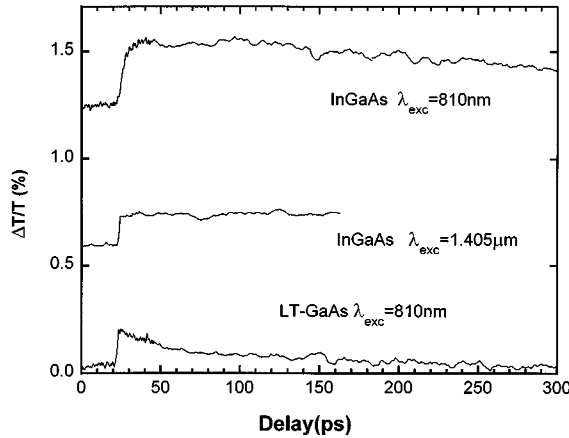

FIG. 2. Long-time temporal dynamics of the spectrally integrated FIR transmission of $In_xGa_{1-x}As$ for two different photoexcitation wavelengths. Absolute differences in response are attributed to photocarrier density differences which are near 5×10^{14} cm^{-3}. The response of low-temperature-grown GaAs is shown for comparison.

is strictly a measure of the carrier density which decreases due to band-to-band recombination or trapping. It is evident from Fig. 2 that the carrier recombination lifetime is somewhat longer than the pulse period of 12 ns, producing the residual carrier density shown. However, the overall recombination rate is independent of excitation photon energy, as shown by the ratio of the peak to minimum ΔT shown in Fig. 2. We have also verified that the carrier dynamics do not measurably change with carrier density over the range of 2×10^{14}–10^{15} cm^{-3}. The different transmission changes shown for the two excitations result from different photoexcitation carrier densities. We also note that THz spectroscopy technique can discern changes in transmission of one part in 10^4. The results for the LT-GaAs depict a $\sim$200-ps recombination lifetime and the subsequent return of the sample conductivity to the quiescent state, and is shown for reference.

We now describe the general features of the conductivity dependence on excess carrier energy within the independent-electron approximation. The effective mass and the momentum scattering rate are the principle parameters which determine the conductivity. Both of these may change dramatically with carrier energy. The carrier densities remain essentially constant at short times. For carriers which remain in a single valley of a band, the effective mass changes in a well-defined manner, generally increasing with increasing energy, and is well described by band nonparabolicities. In contrast, the various momentum scattering mechanisms do not maintain such a simple relation to carrier energy. For LO-phonon-scattering limited transport, carriers experience an increased scattering rate with increasing excess energy $1/\tau_m \propto E^{1/2}$. On the other hand, the rate of ionized impurity scattering depends inversely on carrier energy[10] $1/\tau_m \propto E^{-3/2}$. We note that electron-hole scattering may be approximated as ionized impurity scattering.

If carriers have sufficient energy to scatter to lower mobility satellite valleys, the effective conductivity is drastically reduced by both changes in effective mass and scattering rates. Thus the rise time of the photoconductivity depends on the carrier cooling rate, including the relaxation time for carriers that may scatter to satellite valleys. Importantly, our low photoinjected carrier densities avoid hot phonon and screening effects which dramatically reduce the electron-energy-loss rates.[11]

In Fig. 3(a) the integrated transmission spectra following photoexcitation is shown for excitation wavelengths of 810 nm, 1.38 μm, and 1.52 μm, corresponding to an excess electron energy of 680, 137, and 60 meV, respectively, as measured from the Γ conduction-band minimum. Both valence- and conduction-band nonparabolicities have been included in the estimate of excess electron energy. By measuring the incident power, absorption, and spot size, we estimate that each incident pulse creates carrier densities of 8×10^{14}, 1.6×10^{14}, and 1.1×10^{14} cm^{-3} for the three wavelengths, respectively.

The conductivity rise time observed for 810-nm excitation is dramatically longer than that observed for lower-energy excitations. We attribute this to intervalley scattering, which occurs only for the 810-nm excitation. The energy difference between the lowest satellite valley (L) and the conduction-band minimum is 550 meV. Excitation at 810 nm thus creates carriers $\sim$130 meV above the L-valley minimum. Since the mobility of L-valley electrons is less than one-tenth that of Γ-valley electrons, we ascribe all of the observed conductivity to Γ electrons. Conductivity changes resulting from cooling within the Γ band are small compared to those associated with intervalley scattering. We will show that this energy dependence of the mobility within Γ is modest, so that the rise time of the 810-nm photoconductivity is a direct measure of the intervalley scattering rates.

For the 810-nm excitation, the conductivity rise time is thus a measure of the *net* return of carriers from L to Γ. As pointed out by Stanton and Bailey,[12] the net return of electrons is not simply determined by the L to Γ relaxation time $\tau_{L\Gamma}$, but instead is determined by the cooling rate of carriers within the Γ and L valleys. This arises from the fact that electrons which scatter back to Γ will quickly return to L unless they have cooled to within a LO-phonon energy of the L-valley minimum. This mechanism may be accounted for by modeling the Γ valley as two states. Electrons within the high-energy state may scatter to the single-energy state of the L valley with a rate $\gamma_{\Gamma L}$, and return with a rate $\gamma_{L\Gamma}$. Electrons in the high-energy state of Γ may also scatter to the second low-energy Γ state. Once electrons accumulate in the low-energy Γ state, they are not permitted to scatter to L or back to the high-energy Γ state. The intra-Γ-band scattering rate γ_Δ is determined primarily by the polar-optical-phonon-scattering rate $1/\tau_{LO}$ and the excess energy. For our excess carrier energy, we estimate a γ_Δ of 5×10^{12} s^{-1}. Considerations of detailed balance require that the ratio between $\gamma_{\Gamma L}$ and $\gamma_{L\Gamma}$ be equal to the carrier density ratio between the two states at equilibrium. In the present case this ratio is just equal to the ratio of the density of states (DOS) of the L valley to the DOS of the *upper portion* of the Γ band. It is difficult to determine the corresponding density of states due to the lack of precise band-structure descriptions of $In_xGa_{1-x}As$. However, we estimate that this ratio is close to that calculated for GaAs, which is approximately 10. The resulting coupled differential equations allow the calculation of the temporal dynamics of the occupation of the three

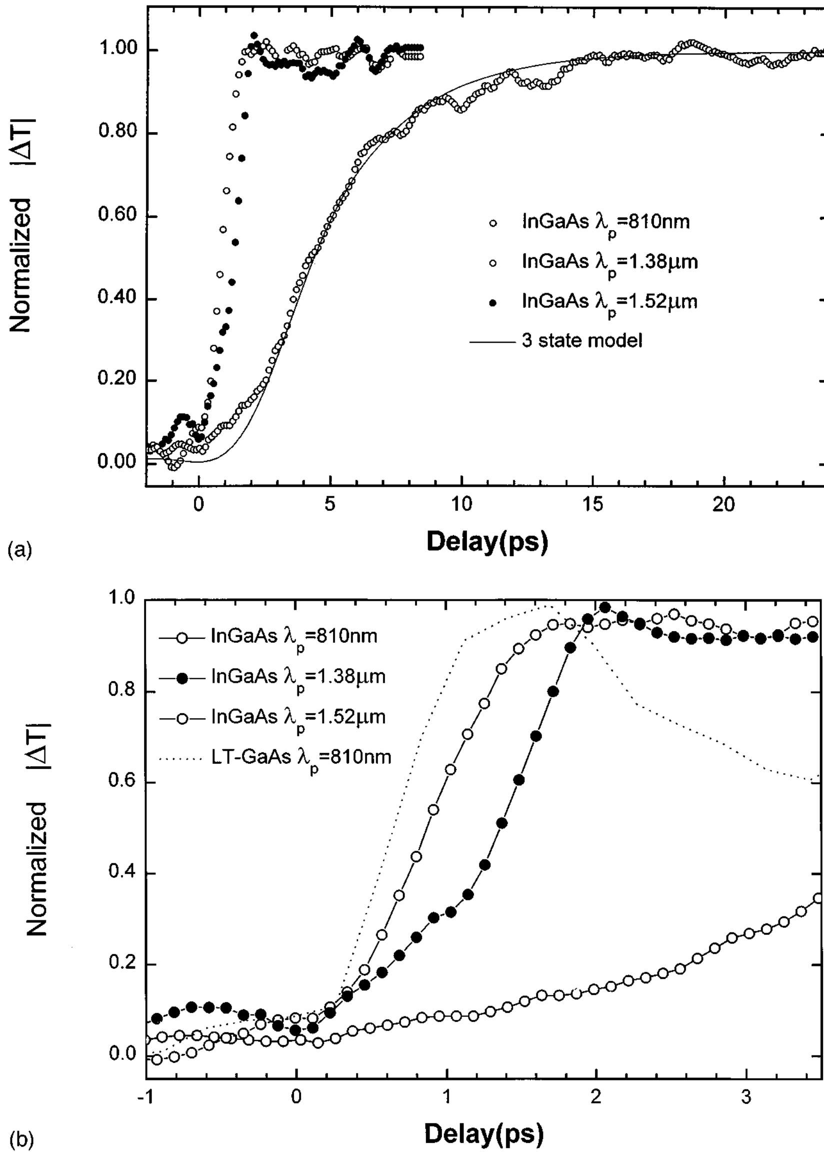

FIG. 3. (a) Normalized transmission change for three distinct excitation energies. The 3.1-ps exponential rise time of the 810-nm excitation results from intervalley scattering and the corresponding long net return time of electrons. The lower-energy excitations exhibit a much faster 0.5-ps rise time attributed to increasing τ_m as carriers cool within the γ band. The solid line depicts the intervalley scattering model appropriate to the 810-nm excitation. (b) Details of the photoconductivity rise time for low-energy excitations. A small decrease in the rise time is observed for 1.5-μm excitation vs 1.38-μm excitation. LT GaAs is shown to have a faster rise time, and depicts the resolution as better than 0.5 ps.

states. Since we ascribe all of the transient conductivity to Γ-band electrons, the sum of occupancy of both the upper and lower Γ-band states is proportional to the conductivity, and hence the transmission change.

In Fig. 3(a) the best-fit results of the three-state model together with the transient transmission data for 810-nm excitation are shown. The corresponding scattering times are $1/\gamma_{L\Gamma}=350$ fs and $1/\gamma_{\Gamma L}=35$ fs. The measured response and the model results are well approximated by an exponential time constant of 3.1 ps. We note that this is shorter than the luminescence rise time data of Shah *et al.* for electrons with $\sim$300-meV excess energy with respect to the L-band minimum in GaAs. Since the time-resolved PL data are heavily weighted with band-edge luminescence, the PL data corresponds to the total cooling time of the band edge, which may be $\sim$1 ps longer than our intervalley relaxation time. The larger excess electron energy and the higher carrier density may also contribute to the observed longer PL rise time.

The effective intervalley return time of 3.1 ps is longer than that reported by Nuss, Auston, and Capasso[13] for GaAs via a similar THz conductivity measurement. In particular we note that Nuss, Auston, and Capasso observed an average exponential return time of $\sim$2 ps for 190-meV excess electron energy above the L-valley minimum, and at a carrier density nearly two orders larger. We believe, therefore, that the $In_xGa_{1-x}As$ L-Γ average return time is generally slower than that of GaAs. The intervalley scattering rate $\tau_{\Gamma L}$ is close to the 30–40 fs reported for GaAs under similar excess carrier energies.[14,15]

The details of the rising edge of the lower-energy excitations are shown in Fig. 3(b). For comparison the conductivity data observed for 810-nm excitation of LT-GaAs is also shown. There is an apparent faster conductivity rise time for lower-energy excitations. Specifically, the deconvolved exponential cooling rates are approximately 0.5 ps for the 1.52-μm excitation and 0.7 ps for the 1.38-μm excitation. In comparison LT-GaAs exhibits a corresponding rise time of 0.4 ps. We make the tentative conclusion that we have observed a faster cooling time associated with the lower-energy excitation. This requires a monotonically increasing τ_m with decreasing carrier energy. We note that, as discussed below, the mobility may be limited by electron-hole scattering events. Thus, when these events are viewed within the framework of ionized impurity scattering, τ_m may not de-

crease with increasing energy. However, the data shown in Fig. 3(b) together with transient transmission data observed at intermediate wavelengths indicate that it is possible to observe these small changes in conductivity rise time associated with changes in excess carrier energy. For excitation insufficient to cause intervalley scattering the observed cooling rates of ~0.7 ps are substantially shorter than that observed for high excess electron energy. Therefore, the 3.1-ps conductivity rise time of the 810-nm excitation corresponds to the intervalley cooling rate.

IV. SPECTROSCOPY

In Fig. 4 we show the results of the second type of measurement, namely, the interferometric determination of the spectral content of the transmitted FIR pulse. The Fourier-analyzed interferometric data at fixed photoexcitation-FIR probe delays for the excitation wavelengths depicted in Figs. 3 are shown in Fig. 4.

The data presented, as well as all of the data observed at various delays, resembles a general Drude-like response. The data observed at a 2-ps delay corresponds to the immediate rising edge of the integrated spectral data of Figs. 3(a). The response at 3 ps is shown in Fig. 3(b) for 1.38-μm excitation. At these short times, the carrier distribution is in a highly nonequilibrium state, and although the overall transmission spectra appears Drude like, these spectra had the largest variation from the best-fit Drude response, which are depicted as solid lines in Fig. 4. In particular, the high-frequency >2-THz conductivity is systematically larger than that of a Drude response. We calculated the transmission response of the photoexcited sample using a multilayer analysis which includes four mediums: air-$In_xGa_{1-x}As$-substrate-air. The fit is heavily weighted for frequencies less than 1.5 THz due to the superior signal to noise in this region. The corresponding mobilities for the best-fit model range from 5000 to 6000 cm^2/V s, which we estimate are accurate to within ± 500 cm^2/V s. The carrier densities of the γ-valley electrons range from 2.5×10^{15} cm^{-3} at 12 ns to 3.4×10^{15} at 16 ps, and are consistent with the excitation parameters and the carrier lifetime data of Fig. 2.

Figure 4(b) shows the corresponding spectrally resolved data for 1.38-μm excitation. These data correspond to somewhat smaller excitation densities, and are generally Drude-like. The Drude fits yield a carrier density commensurate with the experimental parameters. More importantly, the resulting mobilities at longer delays also ranged from 5000 to 6000 cm^2/V s. Thus the transient transmission of the THz of photogenerated electrons yields a mobility which is independent of excitation wavelength as expected.

It has been shown by Vengurlekar and Jha[16] that for specific excess carrier energies and sufficiently narrow excitation energy spread, a dramatic variance from a Drude-like response is expected at very short temporal delays <2 ps. Our data do not exhibit these dramatic variances from the Drude response due to the broad spectral content of our ~50-fs excitation pulses, and to the inability to observe appreciable conductivity changes for delays less than 2 ps.

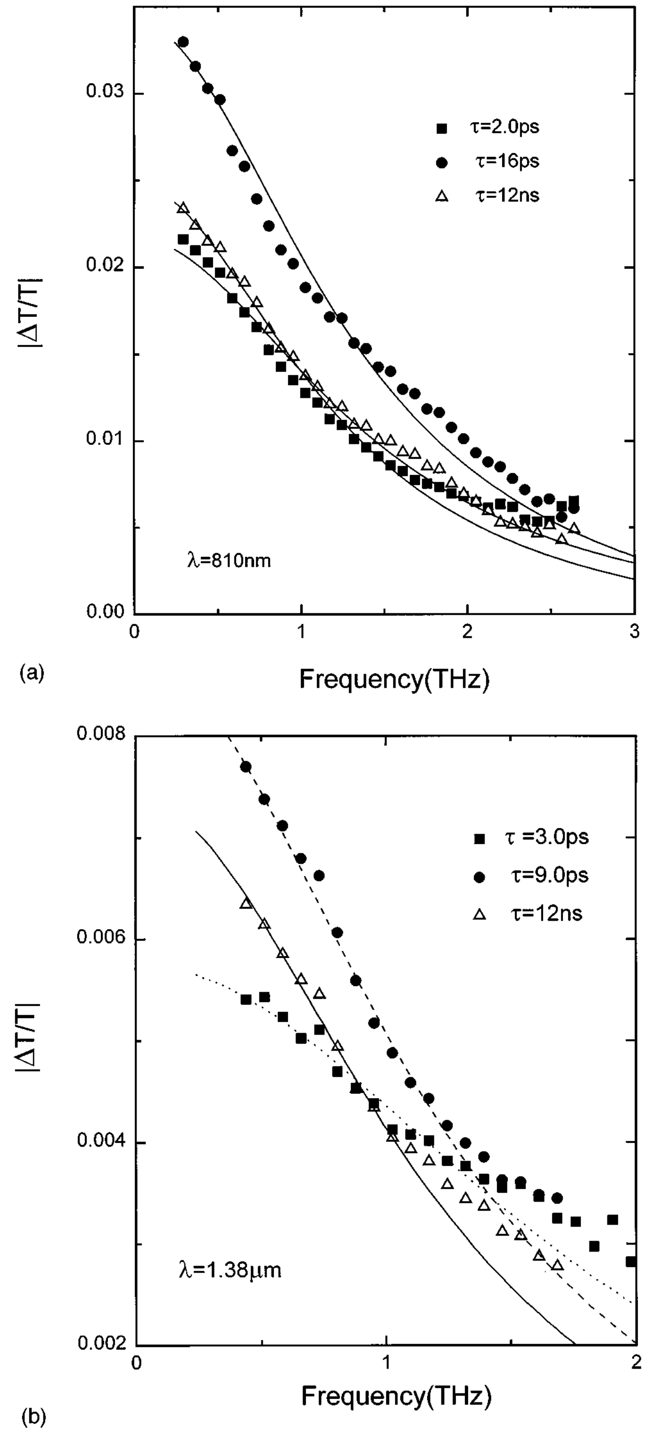

FIG. 4. Frequency dependence of the transmission data for fixed delays between photoexcitation. (a) 810-nm excitation, (b) 1.38-μm excitation. The solid lines represent the best-fit Drude response. In (a) and (b) the mobilities increase from near 5000 to 6000 cm^2/V s as the delay is increased from 2 ps to 12 ns. The corresponding carrier densities are consistent with the measured experimental parameters.

V. DISCUSSION

The Drude-fit mobility, in every case, is less than the Hall mobility, which we measured to be $\mu_H \cong 10\,000$ cm^2/V s. This result was not observed in the static THz conductivity measurements of n- and p-type GaAs, which yielded a

Drude-fit mobility which very closely matches the observed Hall mobility.[17] However, a substantially reduced Drude-fit mobility was observed in GaAs using a related photoexcited THz-probe technique.[6] For large photogenerated carrier densities, this discrepancy between the observed Hall mobility and the FIR photoconductivity has been attributed to the additional momentum relaxation associated with electron-hole scattering events. We note that our observed Drude-fit carrier mobility is less than the factor of 4 observed previously in GaAs.[6] We attribute this to the dilute carrier densities in our experiments. However, for the very dilute carrier densities in the present work, it is difficult to attribute the reduced mobility solely to this mechanism. This can be seen by considering that electron-hole scattering is well approximated by ionized impurity scattering.[18] Thus the observed mobility should be similar to that observed in doped samples with densities equal to the photogenerated carrier density. This interpretation does not reconcile the $\sim$50% mobility reduction observed for carrier densities of $<5\times10^{15}$ cm^{-3}. An additional consideration exists in the present case; the long carrier lifetime results in a distinct equilibrium residual carrier density which is in addition to the highly nonequilibrium photoexcited carrier density. The nonequilibrium photoexcited carriers experience carrier-carrier scattering among themselves as well as with the equilibrium electron-hole distributions.

The Drude model descriptions of the frequency-dependent transmission are well correlated with the observed time-resolved THz spectroscopy data, yielding a carrier density which is consistent with the experimental parameters. The corresponding Drude mobility, on the other hand, is approximately 50–60 % of the separately measured Hall mobility. Thus the observed conductivity is approximately Drude like, even at short times following photoexcitation, although the implied mobility of optically generated carriers is somewhat less than the Hall mobility. We conclude that dilute photoinjected carrier densities yield a photoexcited carrier mobility which is more consistent with the observed Hall mobility than previous THz measurements in GaAs. We have also observed deviations from the ideal Drude response at high frequencies. We attribute the discrepancy between the Hall and Drude-fit mobilities to an enhanced momentum scattering rate which may result from the photoexcitation of impurities and the subsequent increase in ionized impurity scattering.

VI. CONCLUSIONS

In summary, we have measured the carrier cooling dynamics of photoexcited carriers in $In_xGa_{1-x}As$ using terahertz spectroscopy. From the 3.1-ps conductivity rise time the intervalley scattering rate $\tau_{L\Gamma}$ was determined to be 350 fs for carrier densities $\sim10^{15}$ cm^{-3}. Carrier cooling times of $\sim$0.5 ps were observed for photoexcitation, which did not allow intervalley scattering events. The spectrally resolved FIR absorption was modeled using a Drude form of the conductivity with good results. Although deviations at high frequency were observed, particularly at short times after photoexcitation. We have also established the ability of terahertz spectroscopy to observe carrier dynamics of very dilute systems.

ACKNOWLEDGMENTS

We thank A. S. Vengurlekar for valuable discussions. Part of this work was supported by the Georgia Research Alliance.

*Electronic address: seralph@physics.emory.edu

[1] Thomas Elsaesser, J. Shah, Lucio Rota, and Paolo Lugli, Phys. Rev. Lett. **66**, 1757 (1991).

[2] J. Shah, B. Deveaud, T. C. Damen, W. T. Tsang, A. C. Gossard, and P. Lugli, Phys. Rev. Lett. **59**, 222 (1987).

[3] R. G. Ulbrich, J. A. Kash, and J. C. Tang, Phys. Rev. Lett. **62**, 949 (1989).

[4] B. K. Ridley, in *Hot Carriers in Semiconductors Nanostructures*, edited by J. Shah (Academic, New York, 1992), pp. 17–51.

[5] B. B. Hu, E. A. de Souza, W. H. Knox, J. E. Cunningham, M. C. Nuss, A. V. Kuznetsov, and S. L. Chuang, Phys. Rev. Lett. **74**, 1689 (1995).

[6] B. I. Greene, P. N. Saeta, D. R. Dykaar, S. Schmitt-Rink, and S. L. Chuang, IEEE J. Quantum Electron. **28**, 2302 (1992).

[7] S. E. Ralph, S. Perkowitz, D. Grischkowsky, and N. Katzenellenbogen, J. Opt. Soc. Am. B **11** (1994), and other papers in this special Terahertz issue.

[8] S. E. Ralph and D. Grishkowsky, Appl. Phys. Lett. **59**, 1972 (1991).

[9] S. E. Ralph and D. Grischkowsky, in *Photoinduced Space-Charge Effects in Semiconductors: Electro-optics, Photoconductivity and the Photorefractive Effect*, edited by D. D. Nolte, N. M. Haegel, and K. W. Goossen, MRS Symposia Proceedings No. 261 (Materials Research Society, Pittsburgh, 1992), p. 89.

[10] For example, see K. Seeger, *Semiconductor Physics*, 4th ed. (Springer-Verlag, New York, 1989), Chap. 6.

[11] H. Lobentanzer, W. Stolz, J. Nagle, and K. Ploog, Phys. Rev. B **39**, 5234 (1989).

[12] C. J. Stanton and D. W. Bailey, Phys. Rev. B **45**, 8369 (1992).

[13] M. C. Nuss, D. H. Auston, and F. Capasso, Phys. Rev. Lett. **58**, 2355 (1987).

[14] F. Capasso, R. E. Nahory, and M. A. Pollack, Solid State Electron. **22**, 977 (1979).

[15] P. C. Becker, H. L. Fragnito, C. H. Brito-Cruz, J. Shah, R. L. Fork, J. E. Cunningham, J. E. Henry, and C. V. Shank, Appl. Phys. Lett. **53**, 2089 (1988).

[16] A. S. Vengurlekar and S. Jha, Phys. Rev. B **43**, 12 454 (1992).

[17] N. Katzenellenbogen and D. Grishkowsky, Appl. Phys. Lett. **61**, 840 (1992).

[18] R. A. Hopfel, J. Shah, P. A. Wolff, and A. C. Gossard, Phys. Rev. B **37**, 6941 (1988).